JGR Atmospheres

RESEARCH ARTICLE
10.1029/2022JD038352

Fine-Scale Characteristics and Dominant Synoptic Factors of Spring Precipitation Over Complex Terrain of the Southeastern Tibetan Plateau

Yin Zhao[1], Jian Li[1,2], Liwen Ren[3], Nina Li[4], and Puxi Li[1,2]

[1]State Key Laboratory of Severe Weather and Institute of Tibetan Plateau Meteorology, Chinese Academy of Meteorological Sciences, Beijing, China, [2]Research Center for Disastrous Weather Over Hengduan Mountains & Low-Latitude Plateau, CMA, Kunming, China, [3]Public Meteorological Service Center, China Meteorological Administration, Beijing, China, [4]National Meteorological Center, China Meteorological Administration, Beijing, China

Key Points:

- Spring rainfall over the southeastern Tibetan Plateau (SETP) is characterized by frequent nighttime events of long duration
- Dominant synoptic factors evolve from low-level wind in early spring to moisture in late spring, continuously producing rainfall over SETP
- Synoptic factors and complex terrain jointly shape fine features and spatial heterogeneity of the spring rainfall over the SETP

Supporting Information:

Supporting Information may be found in the online version of this article.

Correspondence to:

J. Li,
lij@cma.gov.cn

Citation:

Zhao, Y., Li, J., Ren, L., Li, N., & Li, P. (2023). Fine-scale characteristics and dominant synoptic factors of spring precipitation over complex terrain of the southeastern Tibetan Plateau. *Journal of Geophysical Research: Atmospheres*, *128*, e2022JD038352. https://doi.org/10.1029/2022JD038352

Received 8 DEC 2022
Accepted 16 MAY 2023

Abstract Spring precipitation over the southeastern Tibetan Plateau (SETP) produces more than 34% of annual precipitation, which is comparable to summer precipitation. This pre-monsoon rainfall phenomenon, influenced synthetically by atmospheric circulations and topography, makes the SETP an exception to its surroundings. Here, fine-scale characteristics and typical synoptic backgrounds of this unique phenomenon have been investigated. The spring precipitation over the SETP is characterized by high frequency at hourly scale, with a single diurnal peak at night or early morning. Event-based analysis further demonstrates that the spring precipitation is dominated by long-lasting nocturnal rainfall events. From early to late spring, the dominant synoptic factor evolves from terrain-perpendicular low-level winds to atmospheric moisture, influencing the spatial heterogeneity and fine characteristics of the spring precipitation. The westerly dominated type, featured by lower geopotential height over the TP and enhanced westerlies along the Himalayas, produces limited-area precipitation at those stations located at topography perpendicular to low-level winds. In contrast, the moisture-dominated type is featured by an anomalous cyclone over the Bay of Bengal and induces widespread precipitation around the SETP, which is the leading contributor to the spring precipitation there. Accumulated precipitation amount of long-lasting nocturnal events is the largest under moisture-dominated type, which has a large portion of weak precipitation due to weak thermal instability. Findings revealed in this study complete the picture of spring precipitation influenced by different dominant synoptic factors over the SETP, which deepen the current understanding of the joint influence of circulation and topography on the hydrological cycle of complex terrains.

Plain Language Summary The precipitation over the Tibetan Plateau (TP) is generally considered to be concentrated in summer. However, the southeastern TP (SETP) is an exception, where the spring precipitation is larger or comparable compared to summer precipitation. In this study, we analyzed the fine-scale characteristics and typical synoptic backgrounds of this unique phenomenon. The spring precipitation over the SETP is featured by frequent nighttime rainfall events lasting more than 3 hr. In early spring (March), low-level winds uplifted by topography produce the precipitation over the SETP, while atmospheric water vapor plays a more important role in late spring (May). Atmospheric backgrounds and complex terrain jointly influence the fine-scale characteristics and the range of the spring precipitation over the SETP. Our analysis provides a more completed picture of the spring precipitation over the SETP, which typically reflects the joint influence of atmospheric circulations and complex terrain.

1. Introduction

The Tibetan Plateau (TP) is known as the Asian water tower as its important role in local and downstream hydrological cycle (Immerzeel et al., 2010, 2020; Yao et al., 2022). Precipitation over the TP generally peaks in summer, which attracts constant attention due to its notable contribution to the TP heat source and the consequent influence on the East Asian summer monsoon and South Asian summer monsoon (Duan et al., 2017; Feng & Zhou, 2012; Sun & Liu, 2021; Wu et al., 2015, 2017). However, precipitation over the southeastern TP (SETP), the junction of the Himalaya and Hengduan mountains, gets its first peak in spring, which is different from that over the main body of the TP (Ouyang et al., 2020; Wen et al., 2021; Xiao et al., 2013). This phenomenon of

pre-monsoon precipitation marks the arrival of the first rainy season of China, with critical impact on heat source and local glaciers of the TP (Wen et al., 2021; Yang et al., 2013).

The spring precipitation over the SETP results from the combined influence of circulation and complex topography. In spring, the westerly along the southern margin of the TP is perpendicular to the north-south-oriented Hengduan mountains. The air flow is blocked and lifted by the complex terrain, leading to the precipitation over the SETP (Li et al., 2011; Xiao et al., 2013). The pre-monsoon precipitation there often causes hydrological disasters like floods, landslides and debris flows. An in-depth understanding of spring precipitation over the SETP could promote our cognition of orographic precipitation, and is conducive to disaster prevention and mitigation.

Previous studies have investigated basic features of this phenomenon (Lu et al., 2008; Ouyang et al., 2020; Wen et al., 2021; Xiao et al., 2013; Zhang et al., 1992). It has been found that the spring precipitation over the SETP oscillates with cycles of 8 and 16 years, and its moisture sources are the Arabian Sea and the Bay of Bengal (Lu et al., 2008; Zheng et al., 2010). A recent study has further revealed the interdecadal variation of early spring rainfall over this region is driven by the covariability of the Pacific Decadal Oscillation, Atlantic Multidecadal Oscillation, and Indian Ocean Basin Mode (Wen et al., 2021).

Previous studies are mostly from a perspective of seasonally and regionally averaged analysis. However, the fine-scale characteristics of the spring precipitation over the SETP, which refer to the frequency, intensity, diurnal cycle, and event-duration based on hourly records, are still not clear. It has been shown that these fine-scale characteristics of precipitation are closely related to influence of complex terrain (Li, 2018; Yu et al., 2007). Detailed investigation including hourly characteristics and case-based synoptic background is needed, in order to complete the picture of the spring precipitation over the SETP and further advance the understanding of hydrological cycle in area of complex terrain.

The aim of the study is to investigate the fine-scale characteristics and the dominant synoptic factors of the spring precipitation over the SETP based on hourly in situ records and from a case-based perspective. Data and methods used in this study are introduced in Section 2. The fine-scale characters and synoptic types are illustrated in Section 3. The main results are summarized and discussed in Sections 4 and 5, respectively.

2. Data and Methods

2.1. Data

Following previous study of the spring precipitation over the SETP (Ouyang et al., 2020), this study focuses on March to May as the period of spring season. Hourly precipitation from gauge stations around the southeastern TP is used to investigate fine-scale characteristics of the spring precipitation over the southeast TP. The records are obtained from the National Meteorological Information Center of the China Meteorological Administration with strict quality control (Zhang et al., 2016). The study period of station data is the spring season from 1995 to 2015. The Integrated Multi-satellite Retrievals for GPM V06B (IMERG; Huffman et al., 2015, 2019) is used to reveal the spatial range of the phenomenon of pre-monsoon precipitation. The temporal and spatial resolution for GPM are half hour and 0.1°, respectively. Atmospheric variables, including geopotential height, horizontal winds, total column water vapor and vertically integrated transport of water vapor, from reanalysis data set ERA5 are used to clarify the typical synoptic background when spring precipitation occurs over the southeastern TP (Hersbach et al., 2018, 2020). ERA5 is provided by European Centre for Medium Range Weather Forecasts and has a high horizontal resolution of 0.25°. The study period of GPM and ERA5 is the spring season from 2001 to 2015 unless otherwise specified. In addition, version 7 of TRMM 3A25 from the period of 1998–2012 is used to clarify the property (convective or stratiform rainfall) of the spring precipitation over the SETP (Huffman et al., 2007).

2.2. Methods

The fine-scale characteristics of spring precipitation over the SETP will first be investigated in terms of precipitation amount, frequency and intensity at hourly scale. Following previous studies (Li, 2018; Wang et al., 2011; Xie et al., 2021), amount is derived as the average of accumulated precipitation at all non-missing hours. Frequency is calculated as the ratio of hours with measurable ($\geq$0.1 mm hr^{-1}) rainfall to non-missing hours. Intensity is then defined as the ratio of amount to frequency.

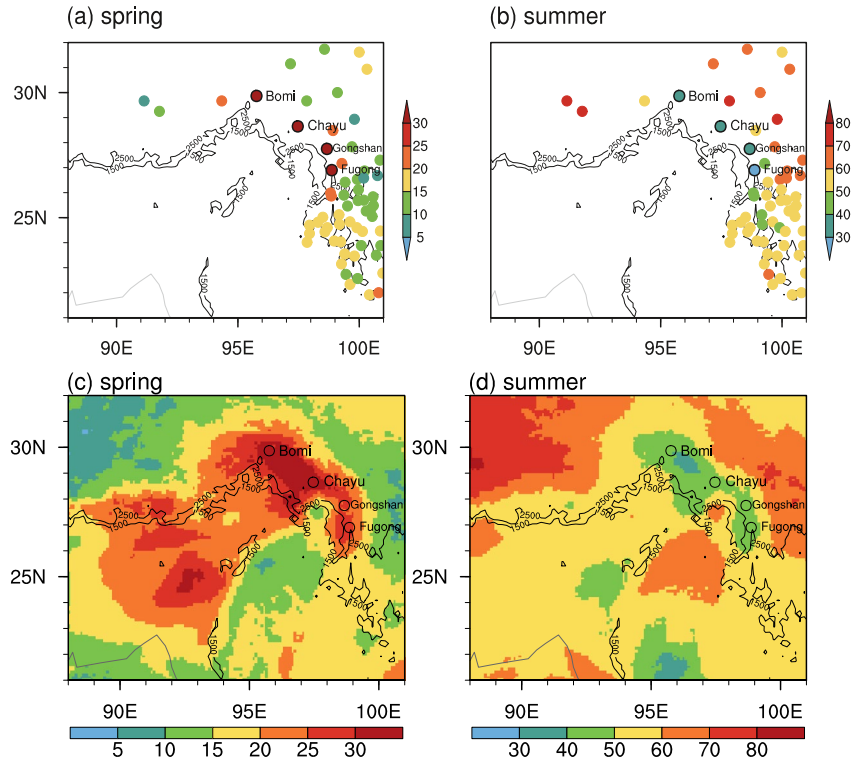

Figure 1. The ratio of spring (panels (a and c), March to May) and summer (panels (b and d), June to August) precipitation to annual accumulation, respectively (%). (a and b) are based on station observation from 1995 to 2015. (c and d) are based on GPM from 2001 to 2020. Black lines indicate terrain of 1,500 and 2,500 m. Circles indicate four typical stations with spring precipitation phenomenon at the southeastern Tibetan Plateau (SETP). Note the ranges between the colorbars of spring and summer are different.

We also explore the fine-scale characteristics of spring precipitation over the SETP through case-based analysis, to investigate the relationship between diurnal cycle and duration of rainfall events from a climatological perspective. Following Yu et al. (2007) and Li (2018), a case or event of precipitation is defined as continuously measurable rainfall with interruption no more than 1-hr. The duration refers to the number of hours between the beginning and the end of event.

To reveal the typical synoptic circulation types of the spring precipitation over the SETP, the self-organizing map (SOM) method is applied (Kohonen, 2001). This clustering method has recently shown its potentials in identifying major patterns of meteorological fields (Dai et al., 2021; Johnson, 2013; Nishiyama et al., 2007; Song et al., 2019). The algorithm of SOM is based on neural network, which projects original data of high dimension onto a lower one. We apply SOM to the daily geopotential height at 500 hPa from 2001 to 2015 in spring, with the climatology removed in advance. When the major types of synoptic circulation have been identified, precipitation events will be affiliated to the corresponding synoptic type according to their beginning time.

3. Results

3.1. Essential Characteristics

Figure 1 shows the contribution of spring and summer (June to August) precipitation to annual accumulation respectively over and around the SETP, based on both gauging and satellite observations. The essential feature of the SETP is that spring precipitation contributes more than 30% to the annual one, while summer precipitation contributes less than 40% (Figures 1a and 1b). This phenomenon is distinct at the windward slope of the mega relief of the SETP, especially represented by four stations named Bomi, Chayu, Gongshan, and Fugong. The consistency between gauging and satellite observations indicates that these four stations could be regarded as representatives for this phenomenon, in order to further investigate the fine-scale characteristics of the spring

Table 1
The Ratio of Spring and Summer Precipitation to Annual Accumulation at the Four Representative Stations (%)

	Spring	Summer
Bomi	39.0	27.5
Chayu	37.9	36.9
Gongshan	35.6	37.6
Fugong	34.0	34.9

precipitation. In addition to the SETP, the contribution of spring precipitation is also above 25% around 90° ~ 94°E, including the central Himalaya, where the pre-monsoon precipitation is observed by ground-based network (Ouyang et al., 2020). However, the contribution of summer precipitation around 90° ~ 94°E is generally still larger than 50% (Figure 1d), which implies the spring precipitation there is not as prominent as that over the SETP.

As shown in Table 1, the contribution of spring precipitation is higher than that of summer precipitation at Bomi and Chayu. At Gongshan and Fugong, the contribution of spring and summer precipitation is comparable. The four typical stations could be regarded as the representatives of the phenomenon of spring precipitation over the SETP.

The topography and climatological circulation of the SETP are shown in Figure 2. As the junction of the west-east oriented Himalayas and the north-south oriented Hengduan Mountains, the SETP is featured by the northwest-southeast oriented terrain. In spring, the climatological westerly along the southern fringe of the TP turns to northwesterly around the SETP. The four representative stations locate at the windward slope of the megarelief and the local winds are perpendicular to the topography. To be specific, at the northernmost Bomi, the west-east oriented terrain is perpendicular to the climatological southerly. Chayu is featured by the northwest-southeast oriented terrain and climatological southwesterly. The southern Gongshan and Fugong are influenced by westerly, which is perpendicular to the north-south oriented terrain. The climatological winds are perpendicular to terrain favors the spring precipitation over the SETP.

3.2. Fine Characteristics at Hourly Scale

On the basis of the cognition of the essential features of the spring precipitation over the SETP, fine characteristics of the spring precipitation are investigated at hourly scale, taking the four typical stations as representatives.

The spring precipitation amount is 3.83, 3.00, 6.12, and 5.86 mm day^{-1}, respectively, at the four representative stations, which is larger than the surrounding stations (Figure 3a and Table 2). There is also distinct difference in precipitation frequency between the four representative stations and the other stations. The frequency of precipitation is larger than 17% at the four representative stations in spring, while it is less than 14% at other stations (Figure 3b and Table 2). The hourly intensity of precipitation decreases from south to north, and there is no distinct difference between the representative stations and other stations of the same latitudes (Figure 3c). It implies that the spring precipitation over the SETP is mainly manifested in the high frequency rather than intensity. In addition, the amount, frequency and intensity of spring precipitation is comparable to that of summer precipitation at the four representative stations (Table 2), corresponding to the considerable contribution of spring precipitation to the annual accumulation of the SETP. The precipitation amount and frequency are the highest at Gongshan, followed by Fugong, Bomi and Chayu (Table 2).

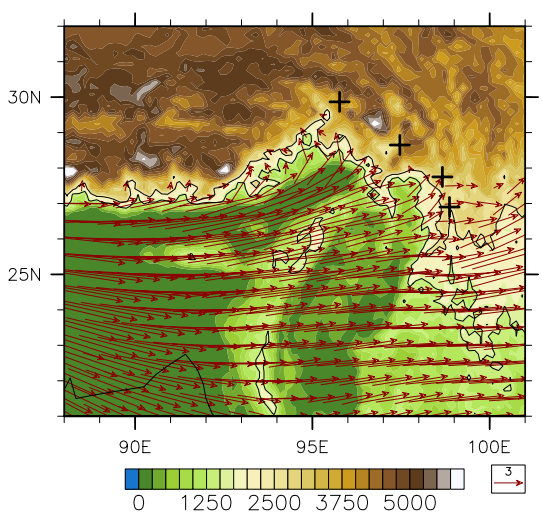

Figure 2. The topography (shading, m) and climatological winds (vectors, m s^{-1}) at 700 hPa in spring over the southeastern Tibetan Plateau. The crosses mark four typical stations.

The diurnal cycle of the spring precipitation at the four representative stations are shown in Figure 4. The precipitation amount peaks singly at night or morning for all representative stations, with the peak time of 4 LST (local solar time), 6 LST, 7 LST, and 7 LST for Bomi, Fugong, Chayu, and Gongshan, respectively. The amplitude of the diurnal cycle of precipitation amount is the largest at Bomi, with a difference of 0.17 mm hr^{-1} between the maximum and minimum. The amplitude of diurnal cycle of precipitation amount is 0.14 mm hr^{-1} at both Fugong and Gongshan, while it is only 0.07 mm hr^{-1} for Chayu. The diurnal cycle of precipitation frequency is generally similar to that of the amount, featured as a major peak of night or morning. Gongshan and Fugong have second peaks in their precipitation frequency at 18 LST and 20 LST, respectively. The similarity between the diurnal cycle of precipitation amount and frequency implies the important role of frequency in the spring precipitation phenomenon over the SETP, corresponding to results

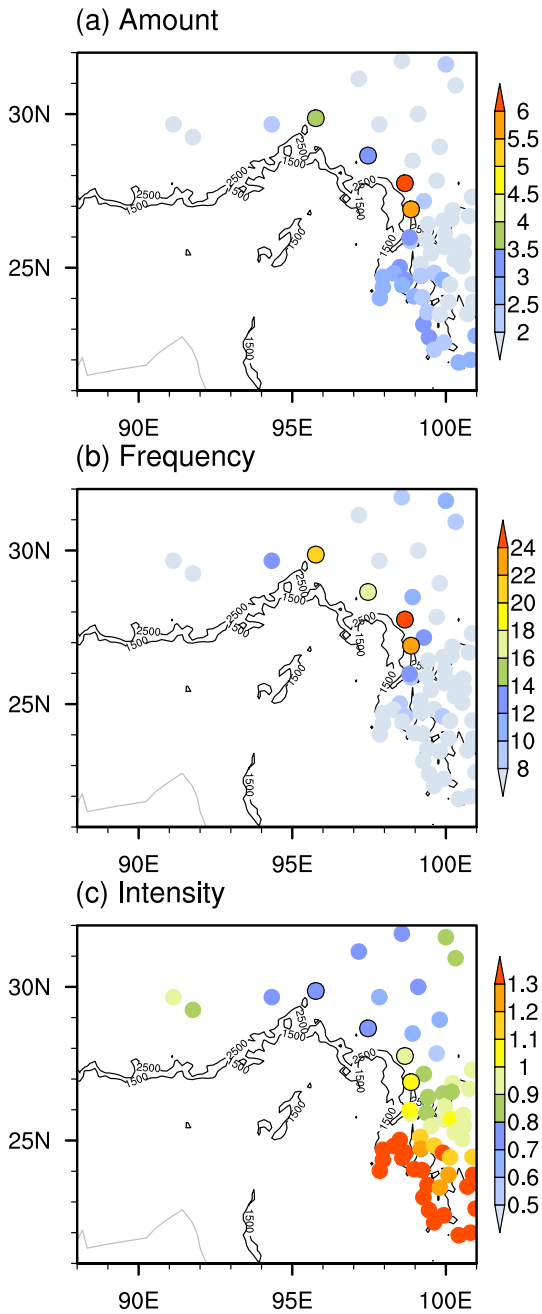

Figure 3. The (a) amount (mm day^{-1}), (b) frequency (%), and (c) intensity (mm h^{-1}) of spring precipitation over the southeastern Tibetan Plateau.

shown in Figure 3. Compared to amount and frequency, the amplitude of the diurnal cycle of precipitation intensity is the smallest. In addition, the diurnal cycle of precipitation intensity shows a main peak at night and a second peak in the afternoon at Bomi, Gongshan and Fugong, while the precipitation is more intense in the afternoon than that at night at Chayu. Overall, the spring precipitation over the SETP is featured by frequent nocturnal rainfall, indicating its relationship with large-scale stratiform precipitation (Li, 2018; Yu et al., 2010).

The relationship between diurnal cycle and duration of spring precipitation events is further investigated. The definition of precipitation events is introduced in Section 2.2, and there are 1220, 2248, 2613, and 2535 events during spring from 1995 to 2015 at four representative stations, respectively. As shown in Figure 5, the case-based accumulation of spring precipitation shows two regions of large value, as the night-to-morning events lasting more than 3 hr and the afternoon-to-evening events with shorter duration. To be specific, the accumulated precipitation at Bomi centers around cases with a peak of 4 LST and lasting 11 hr. The precipitation amount at Chayu centers around night-to-morning (3 LST ~ 8 LST) cases lasting 7 hr and afternoon-to-evening cases (peaks at 21 LST) lasting 3 hr. For Gongshan, the accumulated precipitation features as nocturnal cases with 9-hr duration and evening cases with 4-hr duration. Similarly, spring precipitation events at Fugong have a main center around 6 LST and 7-hr duration, as well as another evening center lasting 4 hr or a little longer. Overall, the spring precipitation over the SETP is dominated by events with long duration. Events lasting 3 hr or more contribute 91.6%, 90.2%, 92.9% and 93.3% to total amount of spring precipitation at Bomi, Chayu, Gongshan, and Fugong, respectively.

Corresponding to Figure 4, the long duration of nocturnal events in Figure 5 also implies non-convective precipitation process. Ratios of stratiform precipitation to total precipitation at four representative stations are 64.0% for Bomi, 77.3% for Chayu, 82.6% for Gongshan and 71.7% for Fugong. Stratiform precipitation has the dominant contribution to the total precipitation compared to convective process, verifying the fine-scale characteristics revealed by hourly precipitation records.

3.3. Typical Synoptic Background and Its Influence

The dominant role of nocturnal events with long duration implies that the main mechanism is about the influence of synoptic background rather than local convective process. In order to reveal the typical synoptic background of the spring precipitation over the SETP, the clustering analysis is applied to atmospheric variables at rainy days. A day is selected as a rainy day when the maximum value of daily precipitation among the four representative stations is larger than 1 mm day^{-1}. There are 930 rainy days selected, accounting for 67.4% of the total 1,380 days of the study period (the spring season from 2001 to 2015). The criterion of rainy day is a trade-off between precipitation intensity and sample size, and the results are not sensitive to this value.

The composited difference in atmospheric circulation and water vapor between the selected rainy days and the climatology is shown in Figure 6. In terms of atmospheric circulation (Figure 6a), the selected rainy days of the spring precipitation are influenced by the anomalous cyclone and low geopotential height at 500 hPa over the TP. The anomalous geopotential height at 500 hPa averaged over the key region (24°N ~ 30°N, 94°E ~ 100°E) of the SETP is −4.4 gpm. Corresponding to the anomalies in geopotential height, anomalous westerly and southwesterly are perpendicular to local topography of the SETP. The average anomalies in zonal and meridional winds at 700 hPa over the key region are 0.6 and 0.4 m s^{-1}, respectively. Regarding the condition of atmospheric

Table 2
The Amount (mm day^{-1}), Frequency (%), and Intensity (mm hr^{-1}) of Spring Precipitation at the Four Representative Stations

	Amount	Frequency	Intensity
Bomi	3.83 (3.48)	21.73 (23.98)	0.73 (0.61)
Chayu	3.00 (2.95)	17.73 (17.23)	0.71 (0.71)
Gongshan	6.12 (6.28)	26.89 (28.20)	0.95(0.93)
Fugong	5.86 (4.13)	23.27 (18.72)	1.05 (0.92)

Note. The corresponding values for summer precipitation are in parentheses.

moisture (Figure 6b), water vapor from oceans of low latitudes is transported toward the SETP by the anomalous southwesterly. The total column water vapor shows positive anomalies along the corridor from the Bay of Bengal to the SETP during the selected rainy days. The anomalous total column water vapor averaged over the key region is 0.9 kg m^{-2}, with the average in anomalous zonal and meridional transport of 19.2 and 11.5 kg m^{-1} s^{-1}, respectively. In general, the spring precipitation over the SETP is favored by the anomalous southwesterly perpendicular to terrain and the related more water vapor in the atmosphere.

In order to reveal more detailed information and dominant factors about the synoptic background of the spring precipitation over the SETP, the anomalous geopotential height at 500 hPa of the selected rainy days is further clustered into four types based on the SOM method (Figure 7). The anomalous geopotential height is positive over the TP and the East Asia, and is negative over the Bay of Bengal in type 1. This type accounts the largest (35.2%) for the clustering rainy days, while it differs from the general composed anomalies shown in Figure 6a. Corresponding to the negative meridional gradient of anomalous geopotential height, there are anomalous easterly winds at 500 hPa over the SETP for type 1, with anomalous zonal winds of −2.8 m s^{-1} averaged over the key region. Type 2 accounts for 24.7% of the total clustering days and is similar to the general composed anomalies, characterized by the negative anomalies in geopotential height over the TP and positive anomalies over the East Asia and the Bay of Bengal. The TP is a center of low geopotential height compared to its surroundings in this type, leading to the anomalous westerlies over the SETP, with anomalous zonal winds of 2.4 m s^{-1} averaged over the key region. As opposed to type 2, the TP in type 3 shows as a center of high geopotential height compared to its surroundings. The anomalous zonal winds are −0.9 m s^{-1} averaged over the key region for type 3, not as significant as those for other types. This type accounts for 20.4% of the total clustering days. In the case of type 4, the anomalous geopotential height is negative over the TP and the East Asia, while it is positive over the Bay of Bengal. This type is generally in contrast to type 2, with positive meridional gradient of anomalous geopotential height at 500 hPa. The anomalous westerly winds are the strongest in this type, which is 4.9 m s^{-1} averaged over the key region. Overall, the clustered types basically indicate the relative changes in geopotential height at 500 hPa between

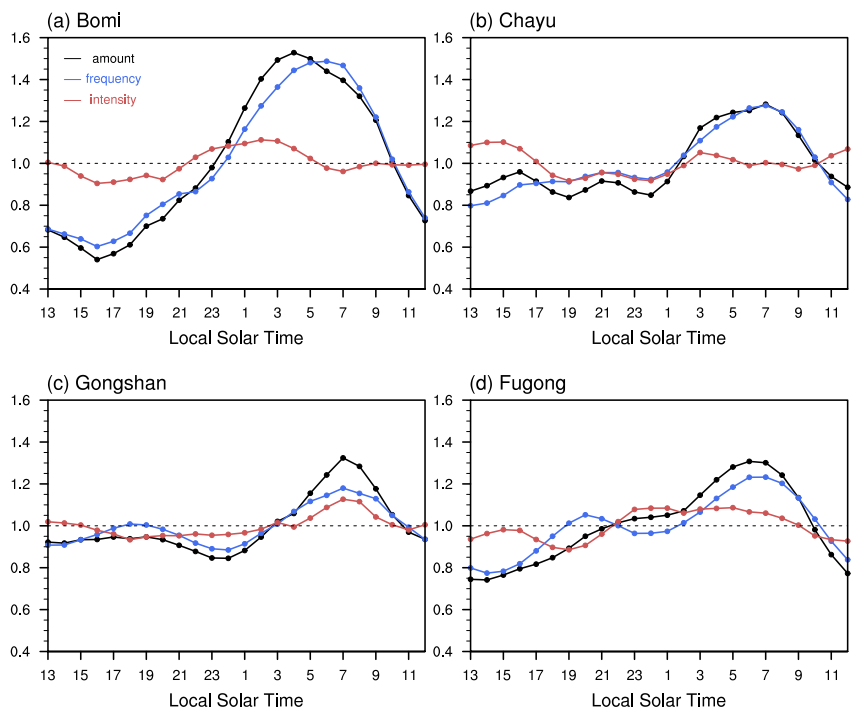

Figure 4. The diurnal cycle of precipitation amount (black lines), frequency (blue lines), and intensity (red lines) in spring at four typical stations. (a) Bomi. (b) Chayu. (c) Gongshan. (d) Fugong. The series is scaled by daily mean value.

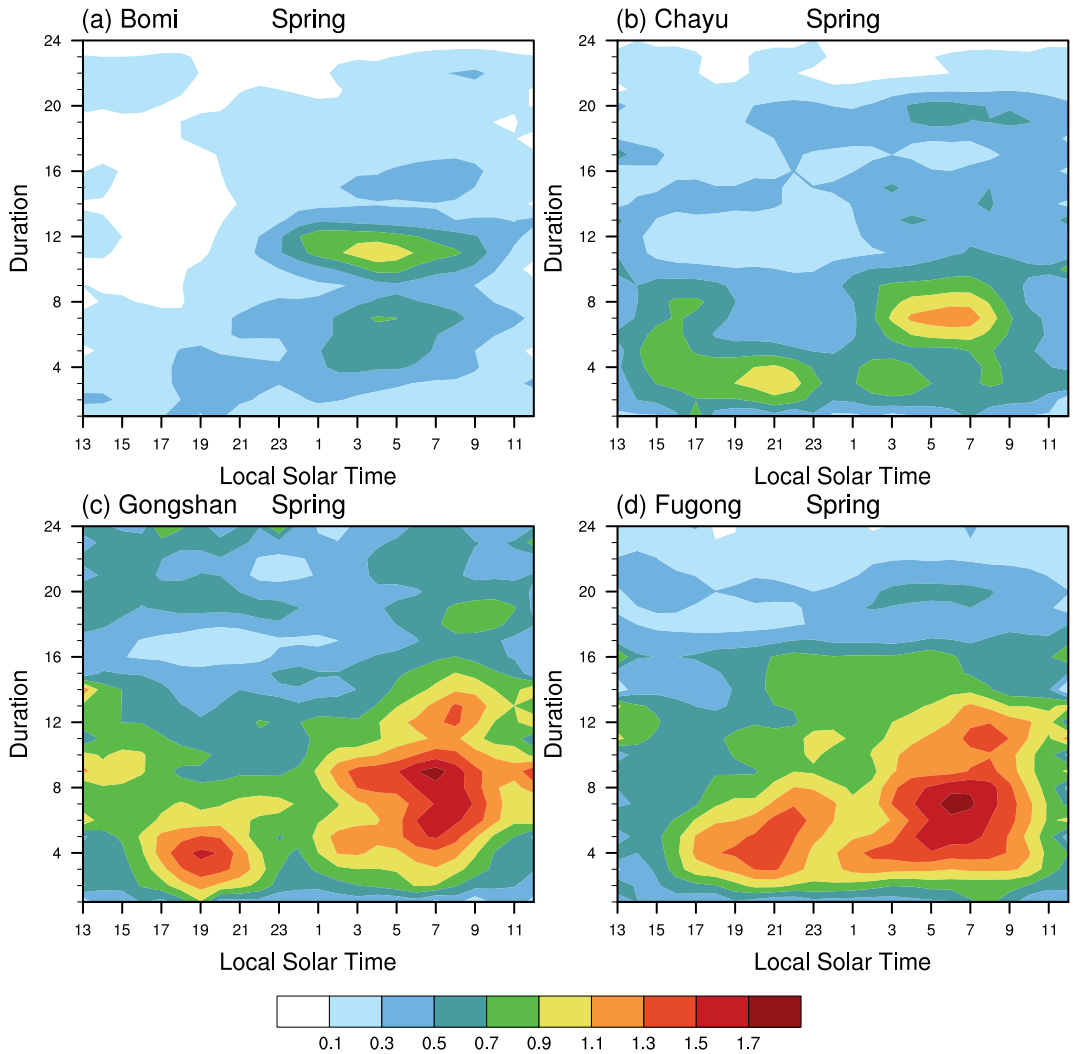

Figure 5. The diurnal cycle of accumulated amount (mm) of spring precipitation cases with different duration. (a) Bomi. (b) Chayu. (c) Gongshan. (d) Fugong.

the TP and its surroundings, which have shown more information about the synoptic background of the spring precipitation over the SETP relative to the general composed analysis of rainy days.

The anomalous circulation at lower troposphere and spatial range of precipitation corresponding to the four synoptic types are further investigated and shown in Figure 8. For type 1, corresponding to the anomalous cyclone at low level of troposphere over the Bay of Bengal, the westerlies decrease while southerlies increase over the SETP. The anomalous zonal and meridional winds averaged over the key region are −1.1 and 0.1 m s^{-1}, respectively. The area of positive anomalies in precipitation is the largest among the four types, with a band of large value along the enhanced southerly winds of the eastern flank of the anomalous cyclone. Type 1 contributes the largest (30.7%) to the total precipitation amount at the four representative stations, and the precipitation increases by 1.8 mm day^{-1} averaged over the key region. For type 2, the anomalous anticyclone at lower troposphere over the Bay of Bengal enhances the southwesterly toward the SETP. The zonal and meridional winds increase by 1.9 and 0.6 m s^{-1} over the key region, respectively. Compared to type 1, the area of positive anomalies in precipitation under type 2 is more concentrated around the SETP, with an increase of 0.3 mm day^{-1} over the key region and the contribution of 28.9% to the total precipitation. In terms of type 3, the southwesterly winds at lower troposphere over the SETP enhance slightly. The anomalous zonal and meridional winds averaged over the key region are 0.6 and 0.3 m s^{-1}, respectively. The area of increased precipitation around the SETP is larger than type 2 but still smaller than type 1, with an increase of 1.1 mm day^{-1} over the key region and the contribution of 21.5% to

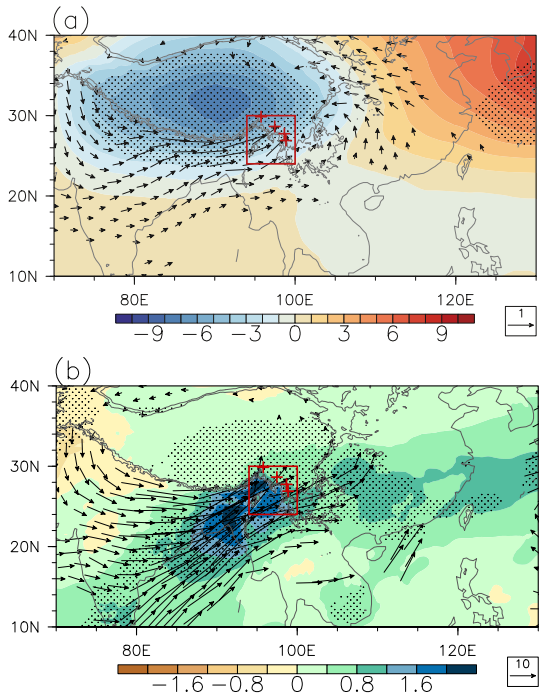

Figure 6. The composited difference between rainy days and climatology. (a) Geopotential height at 500 hPa (shading, gpm) and winds at 700 hPa (vectors, m s^{-1}). (b) Total column water vapor (shading, kg m^{-2}) and its transport (vectors, kg m^{-1} s^{-1}). Dots indicate difference significant at the 90% confidence level. Only vectors significant at the 90% confidence level are shown. Red crosses and rectangle indicate four typical stations and the key area of spring precipitation over the southeastern Tibetan Plateau, respectively.

the total precipitation. The low-level anticyclonic anomalies are the strongest under type 4, which span from the Bay of Bengal to the South China Sea. With the influence of this anomalous anticyclone, there are strong westerlies along the southern fringe of the TP. The zonal and meridional winds over the key region increase by 2.2 and 1.0 m s^{-1}, respectively. The area of increased precipitation under type 4 is the smallest among the four types, limited to area around the representative stations. In addition, the contribution of type 4 to the total precipitation is the smallest (18.9%) among the four types. Regarding the average of the key region, the precipitation decreases by 1.0 mm day^{-1} under type 4.

In addition to anomalies in synoptic circulation, the corresponding background of atmospheric moisture under the clustering types is also investigated. As shown in Figure 9a, water vapor is transported from low-latitude oceans toward the TP in type 1, impacted by the low-level anomalous cyclone and the enhanced southerly winds over the Bay of Bengal. The area of increasing moisture in the atmosphere is the largest for type 1 among the four clustering types, favoring the spring precipitation in terms of precipitable water vapor. In addition, the area of more precipitation along the anomalous southerly winds in Figure 9a corresponds to the largest increase in atmospheric moisture. The atmospheric moisture increases by 4.8 kg m^{-2} averaged in the key region of the spring precipitation over the SETP, resulting from the enhanced zonal (12.0 kg m^{-1} s^{-1}) and meridional (14.4 kg m^{-1} s^{-1}) transport. The total column water vapor decreases by 0.5 kg m^{-2} over the key region for type 2, due to the anomalous anticyclone over the Bay of Bengal. Regarding type 3, the anomalies of atmospheric moisture over the SETP are positive but weaker than that for type 1. The area of negative anomalies in the atmosphere moisture is the largest for type 4 among the four clustering types, indicating a poor condition of moisture for the spring precipitation under this type. As shown in Figure 9d, the total column water vapor decreases by 3.2 kg m^{-2} under type 4, led by the anomalous transport over the Bay of Bengal, which is from land to ocean and away from the TP. Under the background of insufficient moisture, precipitation tends to occur over complex terrain, where the uplift of airflow is strong enough. It may partly accounts for the limited area of precipitation under type 4.

Based on the clustering analysis of the synoptic background, dominant synoptic factors of the spring precipitation over the SETP could be further revealed (Table 3). Given the climatological low-level westerly in spring over the key region, the largest easterly anomalies (−1.1 m s^{-1}) at 700 hPa under type 1 indicate that the background winds are the weakest. However, type 1 has the most abundant water vapor (4.8 kg m^{-2}), implying the dominant factor of atmospheric moisture for type 1. In this monsoon-like case, atmospheric moisture transported by the enhanced southerlies of the anomalous cyclone over the Bay of Bengal plays the key role, and gives rise to broad-area precipitation. In contrast, the least atmospheric water vapor (−3.2 kg m^{-2}) but the strongest low-level westerly winds (2.2 m s^{-1}) imply that type 4 is a westerly dominated type. The dynamic uplift of the enhanced westerly perpendicular to terrain of the SETP is important in terms of this situation, inducing the precipitation process of a limited area. Types 2 and 3 are transitional patterns, and the former has relatively stronger low-level winds. These two typical mechanisms (moisture-dominated type 1 and westerly dominated type 4), as well as their transitions (type 2 and type 3), give rise to the frequent spring precipitation over complex terrain of the SETP. It reflects the synergic influence of variant circulation and complex topography on this unique phenomenon of pre-monsoon precipitation.

The evolution of four synoptic types in spring (March–May) is shown in Figure 10. Type 1 hardly occurs before the seventh pentad, while its frequency increases gradually after that (Figure 10a). The frequency of type 1 peaks around the last pentad in spring, favored by the increasing atmospheric moisture related to the development of South Asian summer monsoon. Inversely, type 4 concentrates before the seventh pentad. The frequency of type 4 is the largest in the first pentad and keeps relatively high values during March, while decreases dramatically after its second peak around the fourth pentad. The evolution of type 1 is corresponding to the prominent zonal winds along the southern TP before the outbreak of South Asian summer monsoon. Type 2 and type 3 concentrate around the medium period of spring pentads, which additionally verifies that they are

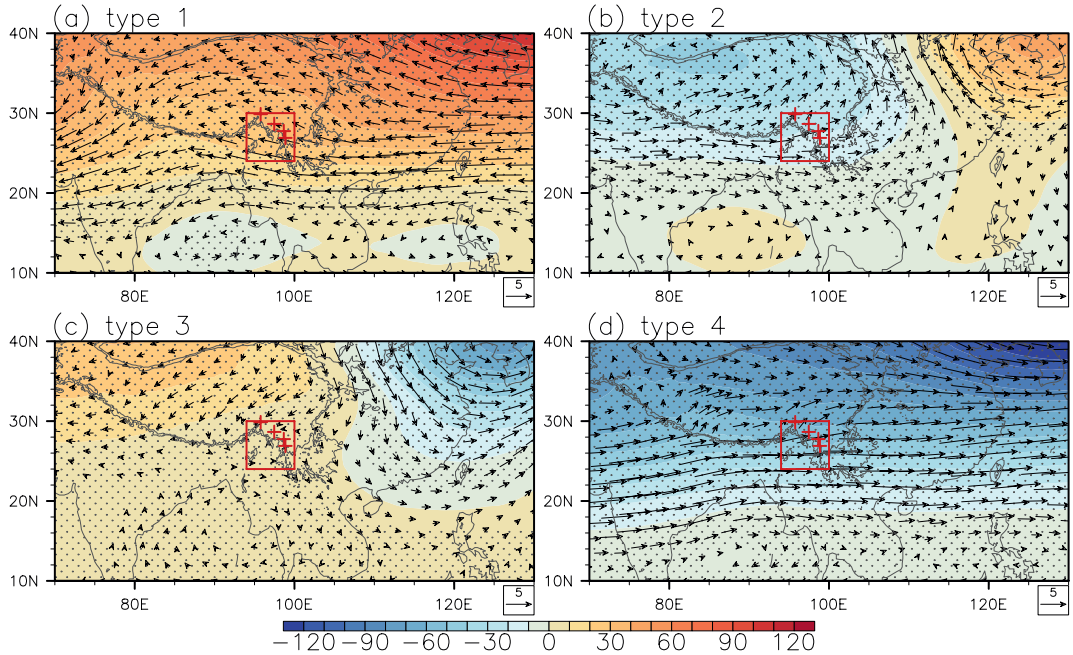

Figure 7. The four types of synoptic circulation classified by the SOM method. Daily anomalies of geopotential height (shading, gpm) and horizontal winds (vectors, m s^{-1}) at 500 hPa relative to climatology for (a) Type 1, (b) Type 2, (c) Type 3, and (d) Type 4. Dots indicate difference significant at the 90% confidence level. Only vectors significant at the 90% confidence level are shown. Red crosses and rectangle indicate four typical stations and the key area of spring precipitation over the southeastern Tibetan Plateau, respectively.

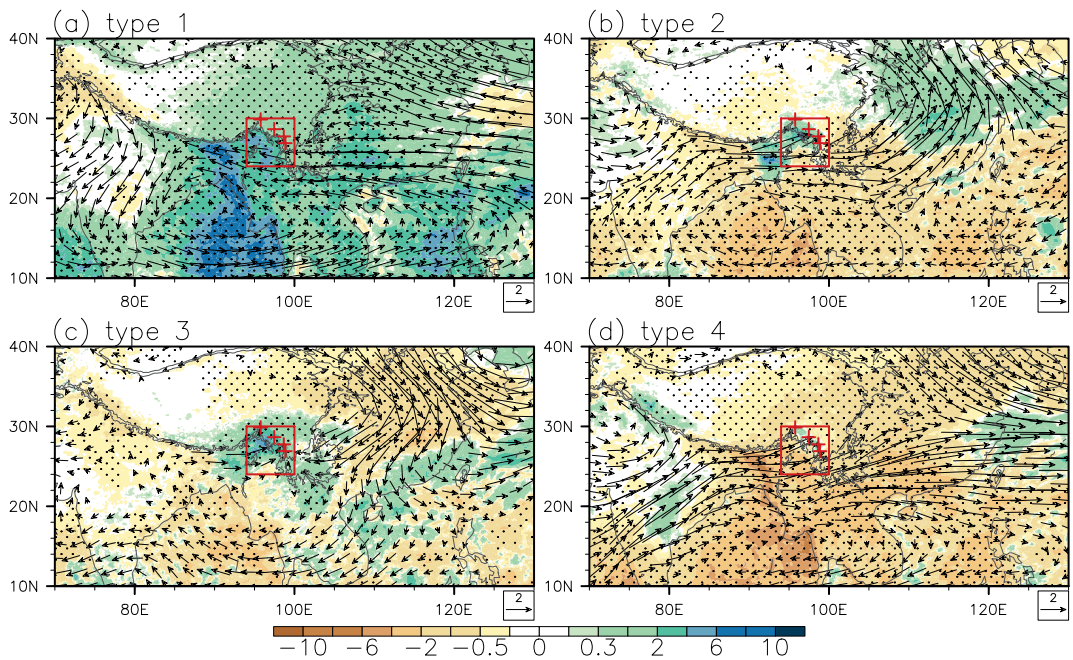

Figure 8. Corresponding anomalies of precipitation (shading, mm day^{-1}) and winds at 700 hPa (vectors, m s^{-1}) under four synoptic types. (a) Type 1. (b) Type 2. (c) Type 3. (d) Type 4. Dots indicate difference significant at the 90% confidence level. Only vectors significant at the 90% confidence level are shown. Red crosses and rectangle indicate four typical stations and the key area of spring precipitation over the southeastern Tibetan Plateau, respectively.

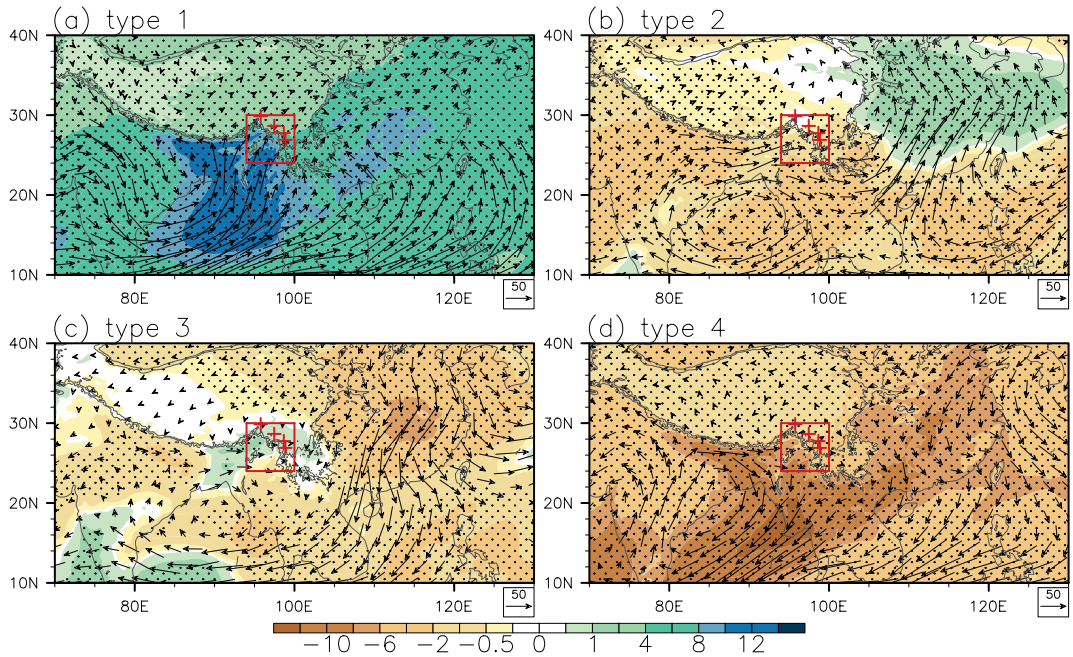

Figure 9. The same as Figure 8, but for total column water vapor (shading, kg m^{-2}) and its transport (vectors, kg m^{-1} s^{-1}). (a) Type 1. (b) Type 2. (c) Type 3. (d) Type 4. Dots indicate difference significant at the 90% confidence level. Only vectors significant at the 90% confidence level are shown. Red crosses and rectangle indicate four typical stations and the key area of spring precipitation over the southeastern Tibetan Plateau, respectively.

transitional types between type 4 and type 1. Type 2 has a prior but minor peak around the third pentad and a major peak around the eighth pentad. The evolution of frequency of type 3 is unimodal, increasing gradually and reaching its peak around the ninth pentad. In general, the synoptic background of the spring precipitation over the SETP shows an evolution of type 4-2-3-1, from the zonal-wind type to the monsoon-like type. As shown in Figure 10b, rainy days of early spring (March) is dominated by type 4 (61.9%), followed by type 2 (24.5%) and type 3 (13.3%). The contribution of type 1 is negligible. The percentages of type 2, type 3, and type 1 in rainy days of April increase to 40.9%, 37.5%, and 18.2%, respectively, while the percentage of type 4 decreases to only 3.4%. In terms of late spring, type 1 accounts for 81.7% of rainy days in May. Type 3 and type 2 contribute 9.5% and 8.9%, respectively, while type 4 has no contribution to the late-spring precipitation over the SETP during the study period. Overall, the synoptic background of the spring precipitation over the SETP evolves gradually from the westerly dominated type in early spring to the moisture-dominated type in late spring. Different synoptic types continuously give rise to the spring precipitation there, leading to its prominent feature of high frequency. This unique phenomenon of pre-monsoon precipitation reflects the comprehensive influence of variant circulation and complex terrain.

The duration and diurnal cycle of precipitation events under different synoptic backgrounds are shown in Figure 11. The precipitation events are affiliated to corresponding synoptic types according to their beginning time. The accumulated precipitation amount of long-duration nocturnal precipitation events is the largest in days of type 1 due to the moist synoptic environment, while that of short-duration evening events is the most prominent in the case of type 2. As a result, the precipitation amount of long-lasting nocturnal events is 2.6 times that of the short-lasting evening events in synoptic type 1, while the ratio is only 2.0 in synoptic type 2. The contribution of precipitation amount under synoptic type 3 and type 4 is smaller compared to that under synoptic type 1 and type 2. The short-lasting evening events in type 2 and type 3 may be related to terrain-induced convection (Kirshbaum et al., 2018; Li, 2018). However, the evening event in type 4 has a longer duration and a later peaking time compared to that in type 2 and type 3, implying its similarity to the non-convective nocturnal events.

Table 3
The Anomalous Zonal Winds (u, m s^{-1}), Meridional Winds (v, m s^{-1}) at 700 hPa, and Total Column Water Vapor (q, kg m^{-2}) Averaged Over the Key Region (24°N ~ 30°N, 94°E ~ 100°E) of the Southeastern Tibetan Plateau Under the Four Synoptic Types

	Type 1	Type 2	Type 3	Type 4
u	−1.1	1.9	0.6	2.2
v	0.1	0.6	0.3	1.0
q	4.8	−0.5	−0.01	−3.2

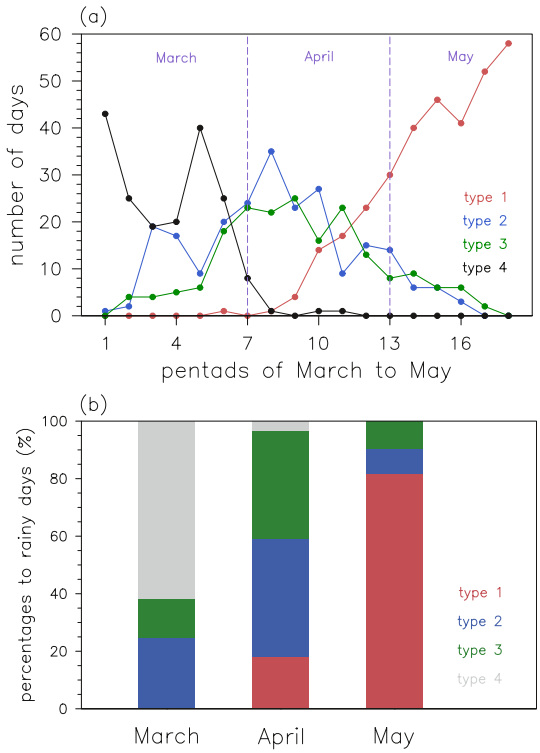

Figure 10. (a) The evolving frequency of four synoptic types in each pentad from March to May. Red, blue, green and black lines represent type 1, 2, 3 and 4, respectively. (b) Percentages of four synoptic types in rainy days for March, April, and May (%). Red, blue, green and gray bars represent type 1, 2, 3, and 4, respectively.

The different characteristics of precipitation events under four synoptic types may refer to the corresponding local thermal instability. The vertical structure of anomalous potential temperature, which is an indicator of the atmospheric thermal instability, is shown in Figure 12. Here we take Bomi as an example and the conditions for the other three stations are the same. As shown in Figure 12a, the lower-to-middle troposphere shows a deep inversion layer under type 1, related to the anomalous warm center at middle troposphere between 300 and 400 hPa. It indicates the weak thermal instability of lower troposphere under type 1. In contrast, there are anomalous cold centers at middle troposphere under types 2 and 3 (Figures 12b and 12c), indicating relatively stronger thermal instability of lower troposphere under these two synoptic types. The anomalous thermal instability of lower troposphere is nearly neutral under type 4 (Figure 12d). In addition, the anomalous difference in potential temperature between 700 hPa and 500hPa averaged over the key region is −0.9 K under type 1, indicating a weaker thermal instability of stratification and prominent nocturnal rainfall. In contrast, the stratification is more unstable for type 2 (0.2 K) and type 3 (0.4 K), favoring the short-lasting events under these two synoptic types. For type 4, the anomalous difference is nearly neutral (0.1 K).

Figure 13 shows the intensity of daily precipitation influenced by different synoptic types. The ratio of days with weak precipitation to the total days is the largest in the case of type 1. The maximum daily precipitation among the four representative stations is weaker than 5 mm day^{-1} for more than 55.4% of the type-1 day, followed by type 3 (44.7%), type 4 (42.1%), and type 2 (39.6%). As the threshold of daily precipitation increases, the ratio in the case of type 1 (red line) decreases rapidly and is gradually lower than other types. The case is the same for the perspective of maximum hourly precipitation (Figure not shown). Only 8.9% of type-1 day have hourly precipitation stronger than 5 mm hr^{-1}, while the corresponding ratios for other types are between 17.0% and 18.0%. The weak intensity of precipitation under type 1 is corresponding to the weak instability of stratification in this case. In addition, Figure 14 also reveals that although anomalous temperature and specific humidity are both higher under type 1 than conditions under other types, the anomalous relative humidity in this case is relatively low, which could be another reason for the large portion of weak precipitation of type 1.

The contribution of different synoptic types is further investigated from the perspective of precipitation at each representative station. As shown in Figure 15a, 50.9% of the spring precipitation at Bomi is related to the synoptic type 1. On the one hand, it is because the spring precipitation at Bomi is featured by nocturnal events of long duration (Figure 5a), which are mainly contributed by the large-area precipitation process related to type 1 (Figure 11a). On the other hand, the enhanced southerly moisture transport toward the SETP in days of type 1 is more likely to give rise to precipitation over Bomi locating at the west-east-oriented terrain (Figure 9a). In general, the contribution of type 4 is smaller than that of other types. Events in days of type 4 mainly influence the precipitation at Gongshan (23.0%) and Fugong (21.4%), which is related to the enhanced low-level westerly along the Himalayas and the north-south-oriented terrain around these two stations.

4. Summary

The spring precipitation over the SETP is a unique phenomenon synthetically affected by atmospheric circulation and complex terrain. Based on hourly rainfall records and the SOM method, the study aims to investigate fine-scale characteristics and the dominant synoptic factors of the spring precipitation there. The results are summarized as follows and shown in Figure 16.

1. The spring precipitation over the SETP shows high frequency at hourly scale. The diurnal cycle of its precipitation amount and frequency peaks singly at night or early morning. Further event-based analysis reveals it is dominated by nocturnal events of long duration (lasting 3 hr or more).

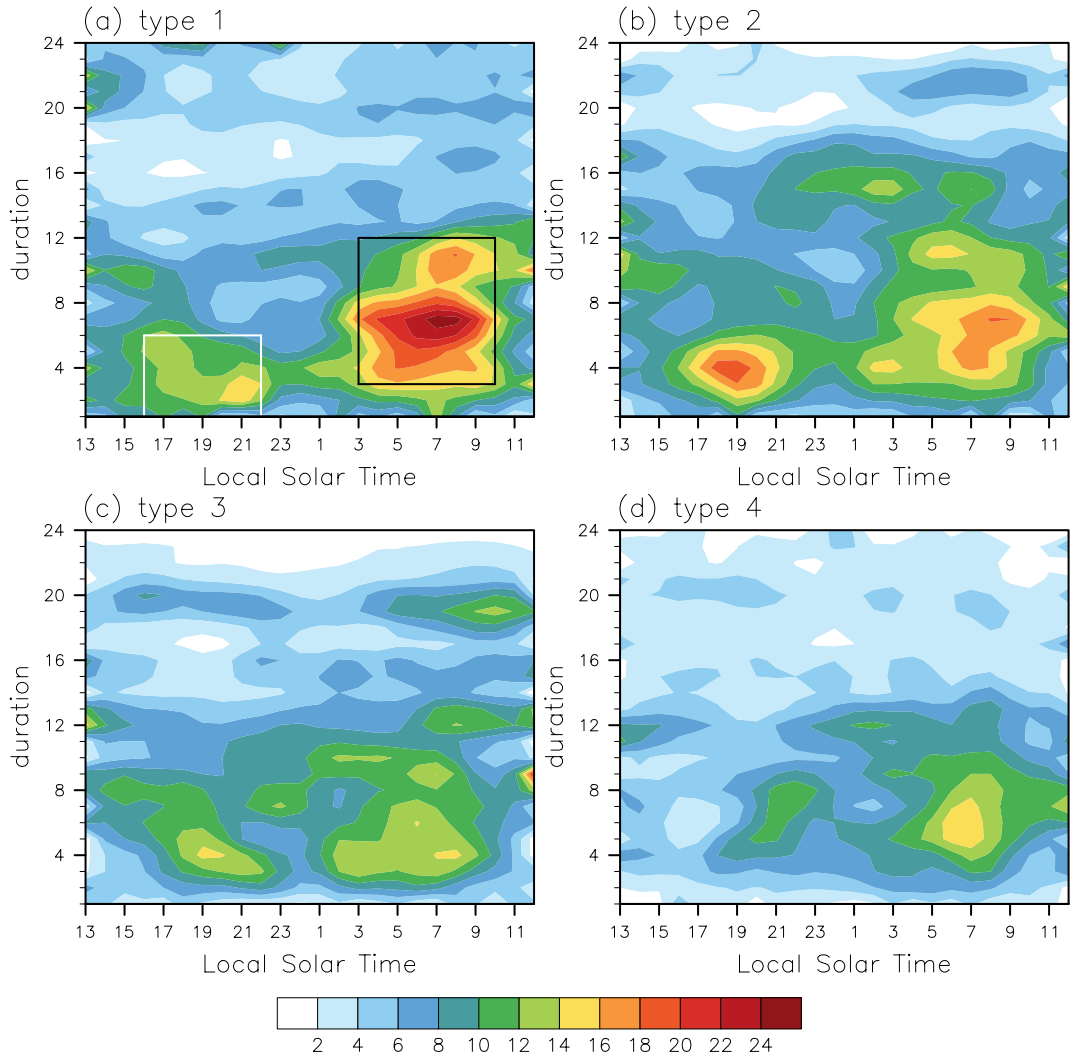

Figure 11. The diurnal cycle of accumulated amount (mm) of spring precipitation cases under four synoptic types. (a) Type 1. (b) Type 2. (c) Type 3. (d) Type 4. The black (white) rectangle in (a) represents the long-lasting nocturnal (short-lasting evening) precipitation.

2. Although westerly prevails over the TP in spring, more details about the typical synoptic backgrounds and the dominant factors of the spring precipitation over the SETP are revealed. In early spring, the low-level westerlies along the Himalayas enhance and cause the limited-area precipitation over the SETP under the background of anomalous low pressure over the TP. Low-level winds uplifted by topography play the key role in this case. In contrast, the precipitation process of a broader area tends to occur over the SETP in late spring, when the anomalies in circulation at lower troposphere over the Bay of Bengal are cyclonic and the atmospheric moisture is abundant. Moisture is the dominant factor for this monsoon-like synoptic type. The dominant synoptic factors evolve from westerly type in early spring to moisture-type in late spring, continuously giving rise to the frequent precipitation over the SETP in spring.
3. Synoptic environments affect the fine-scale characteristics of the spring precipitation over the SETP. The accumulated precipitation amount of long-lasting nocturnal events is the largest under the moisture-dominated type because of its high frequency, while it has a large portion of weak precipitation due to the weak thermal instability. This monsoon-like synoptic type generates more than half of the spring precipitation over Bomi located at west-east-oriented terrain, since precipitation in this case is related to the enhanced northward transport of atmospheric water vapor. In contrast, the westerly dominated process mainly influences the spring precipitation over Gongshan and Fugong, locating at north-south-oriented terrain. The spatial heterogeneity of the precipitation is the consequence of the joint influence of synoptic factors and complex terrain.

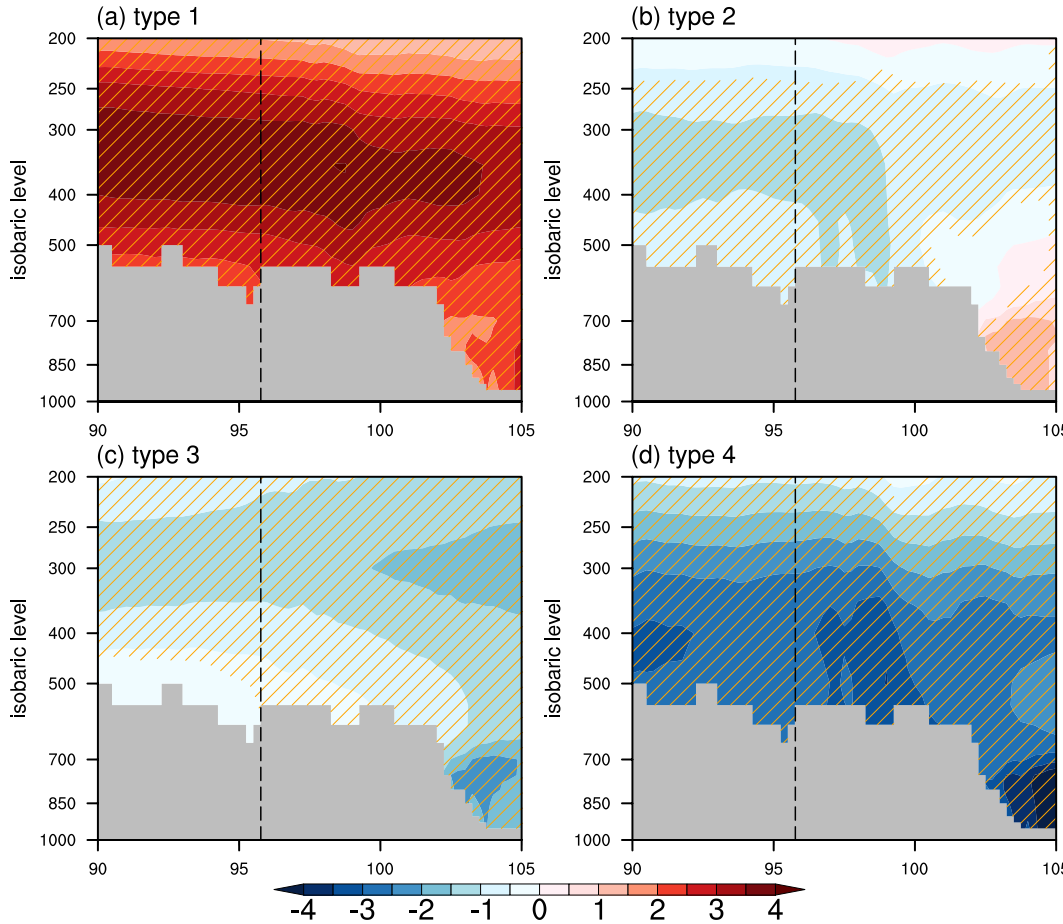

Figure 12. Vertical structure of anomalous potential temperature (shading, K) along the latitude of Bomi under four synoptic types. (a) Type 1. (b) Type 2. (c) Type 3. (d) Type 4. Orange slashes indicate difference significant at the 90% confidence level. Black dashed lines indicate the longitude of Bomi.

5. Discussion

The precipitation over the TP is generally considered to be concentrated in summer. However, the SETP of the transition region between the Himalayas and the Hengduan Mountains is an exception, where the precipitation in spring is larger or comparable compared to that in summer. From the perspective of the evolution of dominant synoptic factors and the joint effect of complex terrain, the reason for this unique phenomenon is revealed in this study, promoting our understanding of the hydrological cycle of this region (Zhao et al., 2022).

The fine characteristics of precipitation crucially impact the land-atmosphere interaction and hydrological cycle over the SETP. On the one hand, different intensity of precipitation influences the water partitioning of the land surface processes (Hu et al., 2020). For instance, intense precipitation contributes to soil moistening and more surface runoff, which may generate disasters like floods, while weak precipitation tends to be evaporated and increase the risk of droughts. Considering the frequent meteorological disasters happened there, the fine characteristics of the spring precipitation over the SETP revealed in this study are conducive to the water resource management and disaster prevention. On the other hand, previous conditions of soil moisture have further influence on the subsequent precipitation through the soil moisture-precipitation feedback (Froidevaux et al., 2014; Guillod et al., 2015; Hu et al., 2021), providing additional predictability for summer precipitation over the SETP.

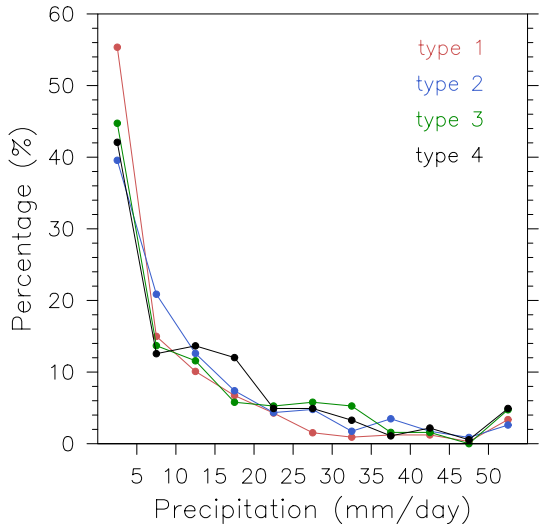

Figure 13. The relative frequency of maximum daily precipitation among four typical stations under four synoptic types. The *x*-axis represents different precipitation intervals (mm day^{-1}). The *y*-axis represents the daily frequency of precipitation scaled by total number of days under the corresponding synoptic type (%). Red, blue, green and black lines indicate type 1, 2, 3 and 4, respectively.

The clustering results of synoptic patterns regarding rainy days essentially reflect the modulation of the geopotential height over the TP compared to that over regions to its east (the East Asia) and south (the Bay of Bengal), in terms of the low-level winds and atmospheric moisture over the SETP. To be specific, the higher (lower) geopotential height over the TP (the Bay of Bengal), the stronger moisture transport and larger area of precipitation. Otherwise, the area of precipitation tends to be limited due to the enhanced westerlies. From the perspective of the comparison between the TP and the East Asia, taking type 2 and type 3 in Figure 7 as examples, lower (higher) geopotential height over the TP (the East Asia) is conducive to giving rise to the enhanced southwesterly and increasing precipitation over the SETP, leading to more precipitation under type 2 compared to type 3 (Figure 11).

Figure S1 in Supporting Information S1 shows the composites of original 700-hPa horizontal winds of the four SOM types. The moisture-dominated type 1 indicates the India-Burma trough pattern (Figure S1a in Supporting Information S1), while the westerly dominated type 4 is manifested as the low-level westerly along the southern TP (Figure S1d in Supporting Information S1). The four SOM types have successfully captured the key features of spring circulation over this region, which is the occasional India-Burma trough under the background of climatological westerly along the southern TP as demonstrated in the previous study (Xiao et al., 2013).

Regarding the sensitivity of results to the number of SOM clusters, Figures S2 and S3 in Supporting Information S1 are two examples of 12 and 16 types. They all reflect the contrast in 500-hPa geopotential height between the TP and its east or south, although with some different details. The number of four types are finally chosen because it could already reflect the main changes in 500-hPa geopotential height over the study region. As shown in Figure S4a in Supporting Information S1, the first EOF mode shows the contrast in 500-hPa geopotential height between the TP and the Bay of Bengal, which is reflected by type 1 and type 4 from SOM. The second EOF mode (Figure S4b in Supporting Information S1) shows that contrast between the TP and the East Asia, which is manifested as type 2 and type 3 from SOM. The first two EOF modes explain 79% of the total variance, implying the contrast between the TP and its east (the East Asia) or south (the Bay of Bengal) is the main component of the change in the 500 hPa geopotential height over the study region.

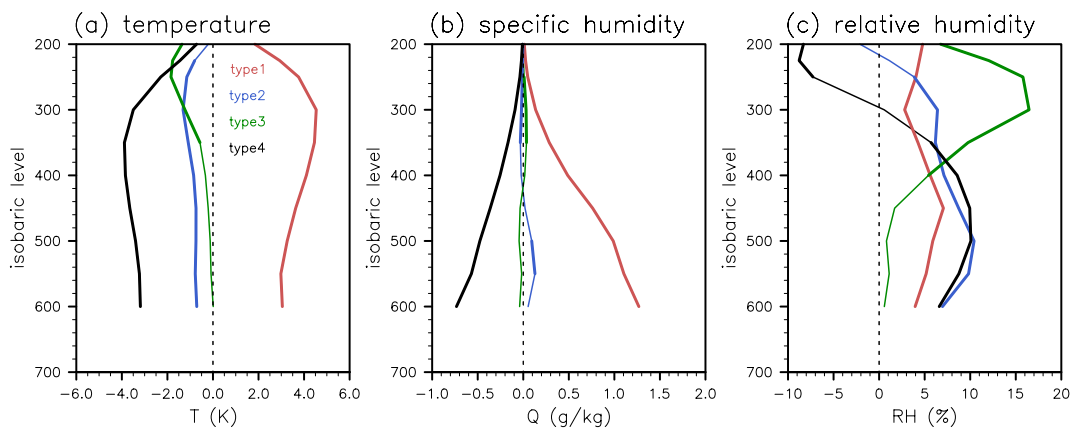

Figure 14. Profiles of anomalous (a) temperature (K), (b) specific humidity (g kg^{-1}), and (c) relative humidity (%) at Bomi under synoptic type 1 (red lines), type 2 (blue lines), type 3 (green lines), and type 4 (black lines). Difference significant at the 90% confidence level is shown with bolder lines.

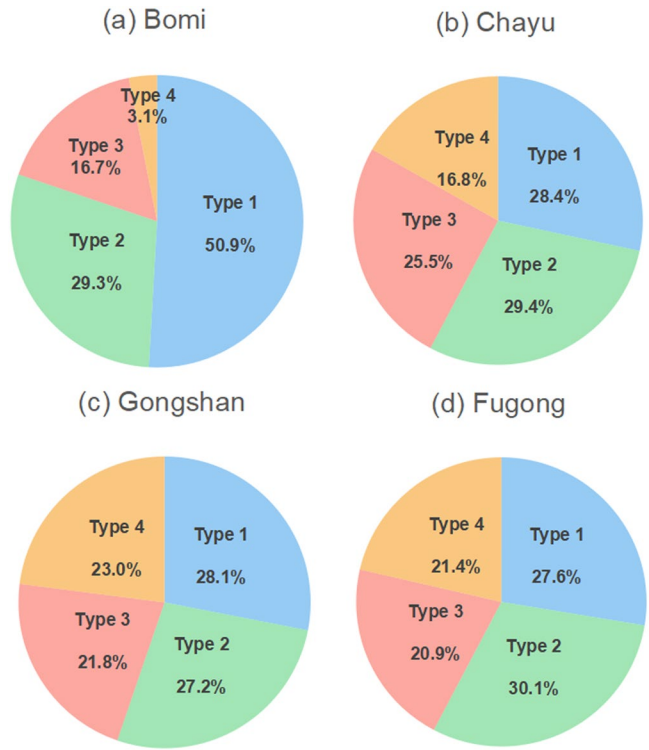

Figure 15. The contribution of precipitation under four synoptic types to total precipitation at four typical stations. (a) Bomi. (b) Chayu. (c) Gongshan. (d) Fugong.

Although the spring precipitation over the SETP is dominated by nocturnal events of long duration, precipitation with earlier peaking time and shorter duration is also revealed through event-based analysis, especially for Gongshan, Fugong, and Chayu (Figure 5). These precipitation events from afternoon to evening may be influenced by the diurnal variance of thermal conditions and surface winds related to local topography (Houze, 2012; Kirshbaum et al., 2018), which could be further investigated by numerical experiments of high resolution, as well as the influence of precipitating diabatic process on the evolution of synoptic circulation. In addition, since orographic precipitation has been a long-lasting challenge for numerical modeling, the fine-scale characteristics and the relevant synoptic patterns of the spring precipitation over the SETP revealed here could provide information for model evaluation and improvement.

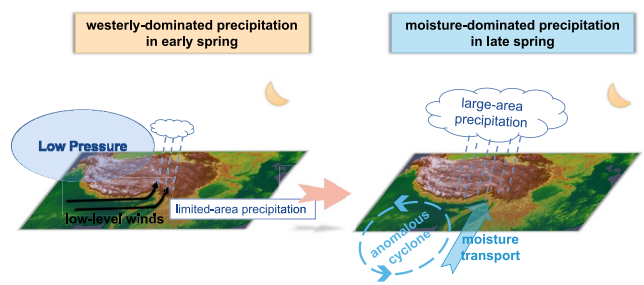

Figure 16. The schematic diagrams of the dominant synoptic factors of the precipitation over the southeastern Tibetan Plateau from early to late spring.

Data Availability Statement

The reanalysis data set ERA5 is provided by the European Centre for Medium-Range Weather Forecasts (Hersbach et al., 2018). The satellite datasets are Tropical Rainfall Measuring Mission (2011) and Integrated Multi-satellitE Retrievals for GPM V06B (Huffman et al., 2019), respectively. Gauging observations can be obtained from the National Meteorological Information Center (Zhang et al., 2016).

Acknowledgments
This work was supported by the National Natural Science Foundation of China (42225505, U2142204, 42205036, 42005039), China Postdoctoral Science Foundation (2022M723469), and the Jiangsu Collaborative Innovation Center for Climate Change. Great gratitude is owed to Dr. Wei Sun for providing the underlying graph of the schematic diagrams.

References

Dai, L., Cheng, T. F., & Lu, M. (2021). Define East Asian monsoon annual cycle via a self-organizing map-based approach. *Geophysical Research Letters*, *48*(1), e2020GL089542. https://doi.org/10.1029/2020GL089542

Duan, A., Sun, R., & He, J. (2017). Impact of surface sensible heating over the Tibetan plateau on the Western Pacific subtropical high: A land–air–sea interaction perspective. *Advances in Atmospheric Sciences*, *34*(2), 157–168. https://doi.org/10.1007/s00376-016-6008-z

Feng, L., & Zhou, T. (2012). Water vapor transport for summer precipitation over the Tibetan Plateau: Multidata set analysis. *Journal of Geophysical Research*, *117*(D20), D20114. https://doi.org/10.1029/2011jd017012

Froidevaux, P., Schlemmer, L., Schmidli, J., Langhans, W., & Schär, C. (2014). Influence of the background wind on the local soil moisture–precipitation feedback. *Journal of the Atmospheric Sciences*, *71*(2), 782–799. https://doi.org/10.1175/jas-d-13-0180.1

Guillod, B., Orlowsky, B., Miralles, D., Teuling, A. J., & Seneviratne, S. I. (2015). Reconciling spatial and temporal soil moisture effects on afternoon rainfall. *Nature Communications*, *6*(1), 6443. https://doi.org/10.1038/ncomms7443

Hersbach, H., Bell, B., Berrisford, P., Biavati, G., Horányi, A., Muñoz Sabater, J., et al. (2018). ERA5 hourly data on pressure levels from 1979 to present [Dataset]. Copernicus Climate Change Service (C3S) Climate Data Store (CDS). https://doi.org/10.24381/cds.bd0915c6

Hersbach, H., Bell, B., Berrisford, P., Hirahara, S., Horányi, A., Muñoz-Sabater, J., et al. (2020). The ERA5 global reanalysis. *Quarterly Journal of the Royal Meteorological Society*, *146*(730), 1999–2049. https://doi.org/10.1002/qj.3803

Houze, R. A. (2012). Orographic effects on precipitating clouds. *Reviews of Geophysics*, *50*(1). https://doi.org/10.1029/2011rg000365

Hu, H., Leung, L. R., & Feng, Z. (2020). Understanding the distinct impacts of MCS and non-MCS rainfall on the surface water balance in the Central United States using a numerical water-tagging technique. *Journal of Hydrometeorology*, *21*(10), 2343–2357. https://doi.org/10.1175/jhm-d-20-0081.1

Hu, H., Leung, L. R., & Feng, Z. (2021). Early warm-season mesoscale convective systems dominate soil moisture-precipitation feedback for summer rainfall in central United States. *Proceedings of the National Academy of Sciences of the United States of America*, *118*(43), e2105260118. https://doi.org/10.1073/pnas.2105260118

Huffman, G. J., Bolvin, D. T., Braithwaite, D., Hsu, K., Joyce, R., Xie, P., & Yoo, S.-H. (2015). NASA Global Precipitation Measurement (GPM) integrated multi-satellite retrievals for GPM (IMERG). *Algorithm theoretical basis document, V06B*, *4*, 30.

Huffman, G. J., Bolvin, D. T., Nelkin, E. J., Wolff, D. B., Adler, R. F., Gu, G., et al. (2007). The TRMM Multisatellite Precipitation Analysis (TMPA): Quasi-global, multiyear, combined-sensor precipitation estimates at fine scales. *Journal of Hydrometeorology*, *8*(1), 38–55. https://doi.org/10.1175/jhm560.1

Huffman, G. J., Stocker, E. F., Bolvin, D. T., Nelkin, E. J., & Tan, J. (2019). GPM IMERG final precipitation L3 half hourly 0.1degree x 0.1degree V06 [Dataset]. Goddard Earth Sciences Data and Information Services Center (GES DISC). https://doi.org/10.5067/GPM/IMERG/3B-HH/06

Immerzeel, W. W., Lutz, A. F., Andrade, M., Bahl, A., Biemans, H., Bolch, T., et al. (2020). Importance and vulnerability of the world's water towers. *Nature*, *577*(7790), 364–369. https://doi.org/10.1038/s41586-019-1822-y

Immerzeel, W. W., Van Beek, L., & Bierkens, M. (2010). Climate change will affect the Asian water towers. *Science*, *328*(5984), 1382–1385. https://doi.org/10.1126/science.1183188

Johnson, N. C. (2013). How many ENSO flavors can we distinguish? *Journal of Climate*, *26*(13), 4816–4827. https://doi.org/10.1175/JCLI-D-12-00649.1

Kirshbaum, D. J., Adler, B., Kalthoff, N., Barthlott, C., & Serafin, S. (2018). Moist orographic convection: Physical mechanisms and links to surface-exchange processes. *Atmosphere*, *9*(3), 80. https://doi.org/10.3390/atmos9030080

Kohonen, T. (2001). *Self-organizing maps*. Springer.

Li, J. (2018). Hourly station-based precipitation characteristics over the Tibetan Plateau. *International Journal of Climatology*, *38*(3), 1560–1570. https://doi.org/10.1002/joc.5281

Li, J., Yu, R. C., Yuan, W. H., & Chen, H. (2011). Early spring dry spell in the southeastern margin of the Tibetan plateau. *Journal of the Meteorological Society of Japan*, *89*(1), 1–13. https://doi.org/10.2151/jmsj.2011-101

Lu, Y. B., Xie, M. E., & Fan, B. (2008). Analyses on climatic features and water vapour transportation of rainy center in southeast corner of Qinghai-Tibetan plateau in Spring. *Plateau Meteorology*, *27*(6), 1189–1194.

Nishiyama, K., Endo, S., Jinno, K., Bertacchi Uvo, C., Olsson, J., & Berndtsson, R. (2007). Identification of typical synoptic patterns causing heavy rainfall in the rainy season in Japan by a Self-Organizing Map. *Atmospheric Research*, *83*(2–4), 185–200. https://doi.org/10.1016/j.atmosres.2005.10.015

Ouyang, L., Yang, K., Lu, H., Chen, Y., LazhuZhou, X., & Wang, Y. (2020). Ground-based observations reveal unique valley precipitation patterns in the central Himalaya. *Journal of Geophysical Research: Atmospheres*, *125*(5), e2019JD031502. https://doi.org/10.1029/2019JD031502

Song, F., Feng, Z., Leung, L. R., Houze, R. A., Wang, J., Hardin, J., & Homeyer, C. (2019). Contrasting spring and summer large-scale environments associated with mesoscale convective systems over the U.S. Great Plains. *Journal of Climate*, *32*(20), 6749–6767. https://doi.org/10.1175/jcli-d-18-0839.1

Sun, H., & Liu, X. (2021). Impacts of dynamic and thermal forcing by the Tibetan Plateau on the precipitation distribution in the Asian arid and monsoon regions. *Climate Dynamics*, *56*(7–8), 2339–2358. https://doi.org/10.1007/s00382-020-05593-9

Tropical Rainfall Measuring Mission (TRMM). (2011). TRMM Radar Rainfall Statistics L3 1 month (5 x 5) and (0.5 x 0.5) degree V7. [Dataset]. Goddard Earth Sciences Data and Information Services Center. Retrieved from https://disc.gsfc.nasa.gov/datacollection/TRMM_3A25_7.html

Wang, F., Yu, R., Chen, H., Li, J., & Yuan, W. (2011). Analysis of diurnal variation characteristics of precipitation in Southwest China. *Heavy Rain Disaster*, *30*(2), 117–121.

Wen, D., Yang, Y., & Cao, J. (2021). Interdecadal variation of early spring rainfall over the southeastern edge of the Tibetan Plateau. *Journal of Geophysical Research: Atmospheres*, *126*(1), e2020JD033058. https://doi.org/10.1029/2020JD033058

Wu, G., Duan, A., Liu, Y., Mao, J., Ren, R., Bao, Q., et al. (2015). Tibetan Plateau climate dynamics: Recent research progress and outlook. *National Science Review*, *2*(1), 100–116. https://doi.org/10.1093/nsr/nwu045

Wu, G., Liu, Y., Zhang, Q., Duan, A., Wang, T., Wan, R., et al. (2017). The influence of mechanical and thermal forcing by the Tibetan Plateau on Asian climate. *Journal of Hydrometeorology*, *8*(4), 770–789. https://doi.org/10.1175/jhm609.1

Xiao, C., Yu, R. C., & Yuan, W. H. (2013). Characteristics of the seasonal evolution of precipitation over the central Western part of the Hengduan Mountain. *Acta Meteorologica Sinica*, *71*(4), 643–651.

Xie, Y., Yuan, W., Yu, L., & Hu, X. (2021). Regional differences in hourly rainfall characteristics over the southeastern extension of the Tibetan Plateau. *International Journal of Climatology*, *42*(2), 1–11. https://doi.org/10.1002/joc.7305

Yang, W., Yao, T., Guo, X., Zhu, M., Li, S., & Kattel, D. B. (2013). Mass balance of a maritime glacier on the southeast Tibetan Plateau and its climatic sensitivity. *Journal of Geophysical Research: Atmospheres*, *118*(17), 9579–9594. https://doi.org/10.1002/jgrd.50760

Yao, T., Bolch, T., Chen, D., Gao, J., Immerzeel, W., Piao, S., et al. (2022). The imbalance of the Asian water tower. *Nature Reviews Earth & Environment*, *3*(10), 618–632. https://doi.org/10.1038/s43017-022-00299-4

Yu, R., Xu, Y., Zhou, T., & Li, J. (2007). Relation between rainfall duration and diurnal variation in the warm season precipitation over central eastern China. *Geophysical Research Letters*, *34*(13), L13703. https://doi.org/10.1029/2007GL030315

Yu, R., Yuan, W., Li, J., & Fu, Y. (2010). Diurnal phase of late-night against late-afternoon of stratiform and convective precipitation in summer southern contiguous China. *Climate Dynamics*, *35*(4), 567–576. https://doi.org/10.1007/s00382-009-0568-x

Zhang, K. Y., Ma, Y. X., & Li, Y. R. (1992). Climatic characteristics of rainfall and humidity in the Dulongjiang river watershed and its neighbourhood. *Yunnan geographic environment research*, *4*(1), 77–86.

Zhang, Q., Zhao, Y., & Fan, S. (2016). Development of hourly precipitation datasets for national meteorological stations in China [Dataset]. Torrential Rain Disasters, *35*, 182–186. http://data.cma.cn/en

Zhao, Y., Li, J., & Li, P. (2022). Difference in the atmospheric water cycle over the Hengduan Mountains between wet and dry summers. *International Journal of Climatology*, *42*(10), 1–13. https://doi.org/10.1002/joc.7533

Zheng, J. M., Zhu, H. M., Ren, J. Z., & Zhang, W. C. (2010). Climatic characteristics of "the Rainfall in Spring" over the longitudinal range-Gorge North in Yunnan Province. *Resources Science*, *32*(8), 1478–1485.